What happens when two ruptures collide?

Soumaya Latour[1], François Passelègue[2], Federica Paglialunga[2], Corentin Noël[2], Jean-Paul Ampuero[2]

[1]Université de Toulouse, CNRS, Observatoire Midi-Pyrénées, IRAP, Toulouse, France
[2]Université Côte d'Azur, CNRS, Observatoire de la Côte d'Azur, IRD, Géoazur, Sophia Antipolis, France.

Key Points:

- We present a unique experimental observation of the collision of two mode II rupture fronts.
- The collision radiates interface waves that propagate at the Rayleigh wave speed along the sliding interface.
- Interface waves are also generated when stopping waves enter the sliding area of the opposite rupture.

Corresponding author: Soumaya Latour, `soumaya.latour@univ-tlse3.fr`

Abstract

We investigate the interaction between two rupture fronts as they propagate towards each other and ultimately collide. This phenomenon was observed during laboratory experiments conducted on poly methyl methacrylate (PMMA). Subsequently, we used numerical simulations to elucidate key aspects of these observations and draw broader conclusions. Our findings indicate that the collision of the rupture fronts generates interface waves that propagate along the sliding interface at the Rayleigh wave speed. Additionally, the rupture fronts interact with the starting and stopping S-wave phases radiated by the opposite rupture fronts, which can locally change their velocity and generate additional interface waves. We discuss the implications of these results for understanding earthquake source phenomena.

Plain Language Summary

Earthquakes are caused by sudden and rapid sliding along tectonic faults. Sliding generally begins at a specific location, the hypocenter, and then expands over the fault. The manner in which this expansion occurs determines the properties and severity of the shaking generated by the earthquake. The edge of the slipping zone is called the rupture front. If the rupture front becomes very distorted, it might arrive in an area of the fault from two different sides and coalesce. In this study, we conducted experiments and numerical simulations to understand what happens when two rupture fronts propagate towards each other and collide. We show that the two rupture fronts disappear upon collision, and produce a specific type of wave that propagates along the sliding surface, called interface waves. Both the rupture front and the waves emitted by the opposing rupture front interact, which can alter the rupture front's speed and create additional interface waves. If similar waves were observed during real earthquakes, they could provide valuable information about the friction between fault rocks.

1 Introduction

It has now long been recognized that the physical phenomenon that generates earthquakes is the propagation of shear rupture along fault interfaces (Kostrov, 1964, 1966; Burridge, 1973; Freund, 1972; Madariaga, 1976, 1977; Svetlizky & Fineberg, 2014). The geometrical and temporal complexities of the rupture front propagation control the fre-

quency content of the radiated seismic waves, which is a key component of quantifying seismic hazard.

A primary mechanism of high-frequency radiation is the abrupt change of rupture velocity. Extreme examples are the so-called starting phases and stopping phases that are generated, respectively, when a static rupture instantly starts to propagate (Madariaga, 1977; Rose, 1981) or when a propagating rupture instantly stops (Fossum & Freund, 1975). However, any continuous acceleration or deceleration of the rupture also produces far-field radiation.

The collision of rupture fronts, also called coalescence, merging, or focusing effect, is another mechanism that generates high-frequency radiation. It can occur in several geometrical contexts. The most obvious is the almost-simultaneous nucleation of two ruptures on the same fault, that then propagate toward each other and merge. This phenomenon has been studied in several numerical models (Fukuyama & Madariaga, 2000; Kame & Uchida, 2008). To our knowledge it has never been detected in actual seismic ruptures, nor previously observed in the laboratory. More significantly, the collision of rupture fronts can also arise from the presence of heterogeneities on the fault (Day, 1982; Das & Kostrov, 1983; Fukuyama & Madariaga, 2000; Dunham et al., 2003). Ruptures can skip or bypass certain zones (e.g., frictional or stress barriers) before rupturing them simultaneously from both sides. In 1D fault models, this leads to a collision in the middle of the barrier/asperity. In 2D fault models, it leads to a first collision when the rupture front finishes to encircle the barrier, and a second one at the center of the barrier/asperity, when the barrier is broken from all sides. This "double-pincer" process has been identified from seismological observations of real earthquakes (Das & Kostrov, 1983; Beroza & Spudich, 1988; Meng et al., 2018; L. Xu et al., 2024). Finally, a last striking example of rupture collision was detected in the ring fault around a caldera (Wang et al., 2024): in this case, a unique rupture nucleates at one point of the fault, propagates in both directions around the ring fault and finally the two rupture fronts collide.

In this work, we present an experimental observation of two rupture fronts propagating towards each other and ultimately colliding, on a linear interface. This observation fortuitously arose during dynamic rupture laboratory experiments. This scenario offers the opportunity to shed light on the mechanism of far-field radiation by rupture coalescence, and is further elucidated and discussed here through numerical simulations.

2 Experimental observation of two ruptures colliding

We investigate slip events occurring between two plates of PMMA in contact along their long edges, producing a mode II rupture geometry (see Figure 1a and supplementary material text S1 for details).

Each rupture event is recorded by a high-speed camera at 1 million frames per second. The positions of the rupture fronts and the changes in the stress field are revealed through the photoelastic properties of PMMA when viewed under cross-polarized light (Xia et al., 2004; Nielsen et al., 2010; Schubnel et al., 2011; Latour et al., 2013; Paglialunga et al., 2023; Gounon et al., 2022; Ravi-Chandar, 2004).

We track the light intensity changes along a line located 0.8 mm off-fault, and plot them in figures that we call videograms (see Figures 1c, 2, S2). Videograms reveal both the passage of the rupture fronts and the propagation of waves along the fault. Conveniently, in this configuration the relationship between changes in light intensity and local shear stress changes is almost linear (see supplementary material text S1 and S5 and Figures S1 and S7).

Nine successive rupture events were observed during the experiment (numbered from 2 to 10). The videograms (Figures 1b and S2) show that three events nucleate near one edge ($x = 40$ cm) of the fault, and five others near the opposite edge ($x = 0$ cm). Event 5 is remarkable: two ruptures nucleate simultaneously at each edge of the sample, and collide near the fault center. Considering that the rupture events in this setup last for a few hundreds of microseconds, the probability of such a simultaneous double nucleation to occur spontaneously is very low, thus this serendipitous observation provides a unique opportunity to experimentally study the process of rupture collision. The shear stress profiles measured just before and after each event (Figure 1c), and the resulting shear stress drop (Figure 1d), reveal two things. First, the stress drop is maximum near the edge at which each event nucleated. For event 5, there is a maximum stress drop of almost equal value at each side, which shows that just before the event, these two areas were equally close to failure, promoting simultaneous nucleation on both sides of the fault. Secondly, there are two local minima of stress drop near the positions $x = 15$ cm and $x = 23$ cm for almost all events. The videograms corroborate this observation: these two areas can be identified by the small light intensity changes at the end of each event, which reveals a small stress drop at these locations. Remarkably, these two local min-

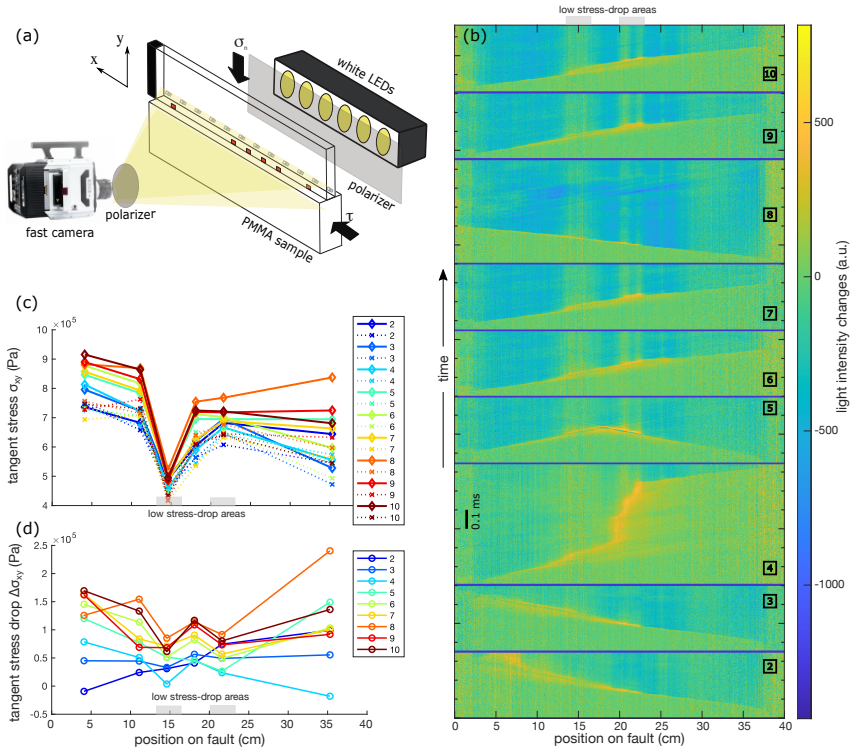

Figure 1. a) Schematic view of the experimental setup CrackDyn located in the Géoazur Laboratory. Stick-slip events are produced at the interface between two PMMA plates, and monitored via photoelasticity with an ultrafast camera, and a network of accelerometers, acoustic sensors and dynamic strain gauges. The friction interface has dimensions of 400 mm × 9 mm and is optically flat. Initially, the samples are brought into contact, and then the upper pistons apply a normal pressure up to 60 bars. This normal pressure is distributed along the entire interface using an aluminum plate, and is kept constant throughout the experiment. Subsequently, a tangential force is gradually applied using a manual pump, leading to a series of slip events. The local strain tensor is measured continuously at 2 MHz at six locations near the fault (red squares) (b) Visualisation of rupture propagation during each slip event. Event number is indicated in each squared label. Blue horizontal lines separates each slip event and correspond to hiatuses in the time axis. Each event is shown separately in Figure S2 of the supplementary material. Events 2, 3 and 8 begin at $x = 40$ cm, events 4, 6, 7, 9 and 10 begin at the opposite edge near $x = 3$ cm. Remarkably, event 5 nucleates simultaneously at both edges of the sample. Two low stress-drop areas acting as barriers are identified (grey). (c) Shear stress profile prior (solid lines) and after (dotted line) each slip event. The event leading to colliding ruptures is event number 5 (see text). The grey areas indicate the approximate locations of the two main stress barriers observed in the videograms. (d) Stress drop profile of each rupture event.

ima of stress drop affect the dynamics of the rupture fronts at these locations. Indeed, a detailed analysis of each rupture front reveals that they decelerate drastically there (see Figure S2).

We focus on event 5 in the rest of this study (Figure 2a). During this event, two rapid ruptures nucleate nearly simultaneously near both fault edges and propagate towards each other. These ruptures propagate at subshear velocities, $v_r = 1180 \pm 10$ m.s^{-1}, and $v_r = 1210 \pm 10$ m.s^{-1}, slightly slower than the Rayleigh wave speed (1258.9 m.s^{-1}) (see supplementary text S4 and Figure S3). At the low stress drop barriers, each rupture significantly decelerates, almost halting for approximately 0.01 ms.

Ahead of each halted rupture front, a negative stress perturbation propagates, initially at the S-wave speed, and then transitions to the Rayleigh wave speed after passing through the opposite rupture front. Following a delay of approximately 0.01 ms, the rupture fronts resume their propagation at sub-Rayleigh wave speeds until they collide at $x = 0.18$ m. Their collision results in their annihilation: the entire fault is sliding at this instant, and there are no more rupture fronts. Nevertheless, a stress perturbation originating from the collision continues to propagate in each direction, at the Rayleigh wave speed. These propagating signals look like a continuation of each rupture front. However, they propagate at the Rayleigh wave speed, faster than the preceding sub-Rayleigh rupture. Moreover, contrary to the rupture fronts, they are not accompanied by a permanent stress drop, but only by a transient negative perturbation of the shear stress.

3 Numerical simulation of colliding ruptures

To interpret these observations, we used the SEM2DPACK spectral element code (Ampuero, 2012) to simulate colliding ruptures in a 2D in-plane geometry. A linear slip-weakening friction law with uniform properties is assumed along the contact interface. A uniform initial normal stress was applied, and the distribution of the initial shear stress was adjusted to simulate two relevant scenarios of colliding ruptures. More details on the numerical parameters are given in supplementary material text S3.

3.1 Two ruptures colliding on a homogeneous fault

We first investigated the case of two colliding ruptures under a *homogeneous initial shear stress* (Figure 3d). We plot the evolution of three simulated fields: the slip ve-

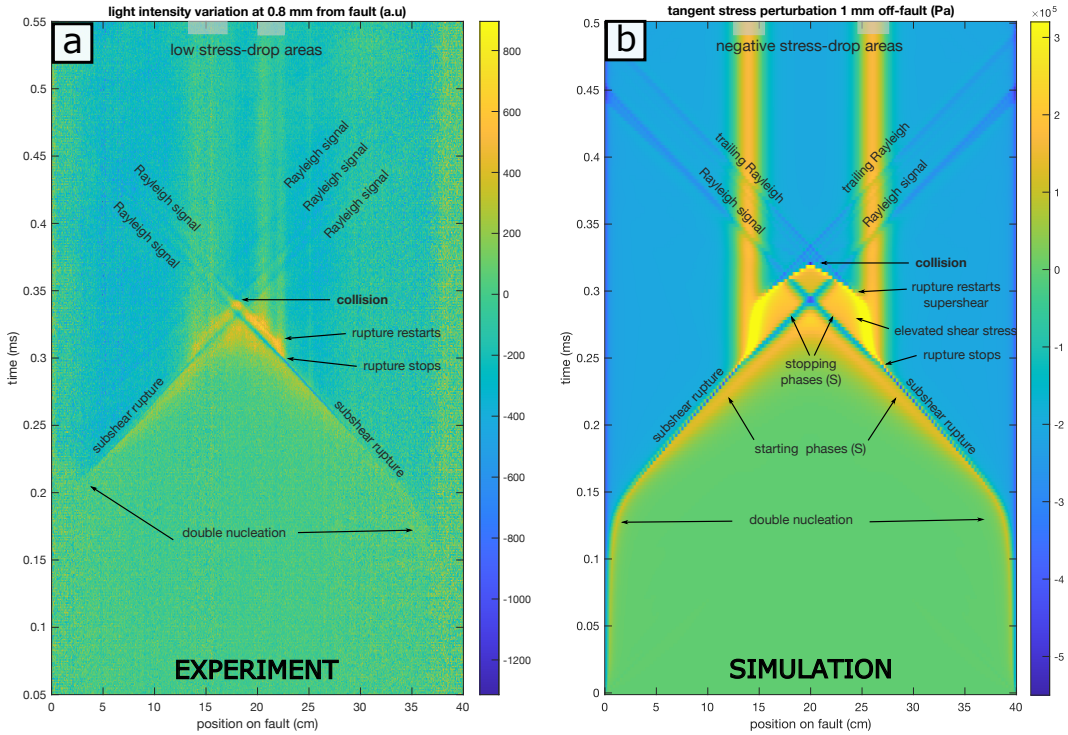

Figure 2. (a) Experimental observation of the collision of two ruptures. Light intensity changes during event 5 along a line of pixels located 0.8 mm above the fault, relative to the local mean value of light intensity during the 20 images that precedes the beginning of the figure. The color scale corresponds to arbitrary units that encode light intensity in the camera, and is proportional to the shear stress change (see supplementary material Figure S1). (b) Simulated shear stress change off-fault in a numerical simulation where two ruptures collide on a fault with two initial stress barriers. This figure is the same as Figure 3g. It has been plotted here for easier comparison with the experiment.

locity (Figure 3a), the shear stress on the fault (Figure 3b), and the shear stress change 1 mm away from the fault (Figure 3c), corresponding to the line of observation of the videogram in the experiment.

The two simulated ruptures start simultaneously on both sides of the fault. After a slow nucleation, they propagate with an almost constant sub-Rayleigh velocity $v_r = 1210 \pm 10$ m.s^{-1} (see supplementary text S4 and Figures S4, S5, S6). Examination of the on-fault shear stress (Figure 3b) before the collision reveals that the rupture fronts are preceded by an increase in stress that corresponds to two distinct effects: (i) a large wavelength ($\simeq 1$ cm) perturbation propagating ahead of the rupture front at the S-wave velocity. This S-wave front is a starting phase radiated by the acceleration of the rupture at the end of the nucleation process. As it propagates faster than the rupture, it separates from the rupture front. (ii) The rupture front itself is preceded by a strong increase at short wavelength, that corresponds to the well-known stress concentration at the rupture tip. Behind the rupture front, the on-fault shear stress drops to the value imposed by the dynamic friction coefficient. Off the fault (Figure 3c), the shear stress changes show similarities with the on-fault stress, but also interesting differences. The long-wavelength pulse due to the leading S-wave is clearly seen. The passage of the rupture front, however, is revealed by a more complex short-wavelength signal than the one observed on the fault.

When the two simulated rupture fronts approach each other, the two preceding S-waves first interfere constructively. This leads to a shear stress higher than the initially imposed shear stress on the fault (Figure 3b). This is the focusing effect described in Fukuyama and Madariaga (2000). Consequently, these rupture fronts propagate on a fault where the stress drop that drives the rupture is locally higher than the one initially imposed. This causes a local and sudden acceleration of the rupture fronts. In fact, close inspection shows that the head of the weakening area transitions to a supershear speed, while its tail continues at sub-Rayleigh speed. At this point, the two supershear head fronts collide, followed by their subshear tails. Both of these collisions locally increase the slip velocity (Figure 3a). Afterwards, the two rupture fronts no longer exists.

However, two types of signals are radiated along the sliding fault by the collision. Signals of the first type carry a peak of slip velocity at the P-wave speed(Figure 3a). Signals of the second type originate from the end of the collision. They look like a contin-

uation of the colliding rupture fronts, but are different in nature and velocity, as discussed in section 4. They are associated with a negative perturbation of the off-fault shear stress (Figure 3c) and a drop in slip velocity propagating at the S wave speed, followed by a peak propagating at the Rayleigh wave speed (Figure 3a). After a while, it triggers a kind of "stick pulse": a "non-slipping" zone that propagates across the sliding interface, widening as it propagates.

The simulated off-fault shear stress (Figure 3d) reproduces well the experimental results (Figure 2a) for the nucleation and the initial fast propagation, especially the positive stress change of the starting S-wave phases, and the short wavelength change attached to the rupture fronts. However, it fails at reproducing the complexities observed in the experiments at the two locations where stress barriers are expected to exist.

3.2 Two ruptures colliding after a delay due to a stress heterogeneity

Two stress barriers were introduced along the fault in a second simulation (Figure 3h). To mimic the effect of the low stress drop areas observed in the experimental event, we had to set the minimum initial shear stress inside the simulated barriers lower than the dynamic strength, resulting in negative stress drop in these areas (Figure 1d).

The initial stages of the simulation are identical to the homogeneous fault case (Figure 3). The ruptures then almost arrest upon entering the barriers. The starting phases continue to propagate at the S-wave speed, followed by a short-wavelength signal indicating negative stress change, which can be identified as the stopping S-wave phases radiated by the strong deceleration of the ruptures at the barriers (Fossum & Freund, 1975; Madariaga, 1977; Dunham & Archuleta, 2004). After these phases pass, the shear stress remains higher than its initial value, due to the establishment of the static field behind the S-wave front.

The two ruptures accelerate again upon exiting the barriers. Due to the elevated shear stress between the barriers, they immediately reach a supershear velocity. This acceleration generates a trailing Rayleigh wave, which follows the ruptures and appears as a propagating peak in sliding velocity (Figure 3e) and a minimum in the off-fault shear stress (Figure 3g). Each rupture then encounters the stopping wave radiated by the opposite rupture front and diffracts it, in a mechanism symmetric to what is described in Dunham and Archuleta (2004). This interaction results in a local and temporary decel-

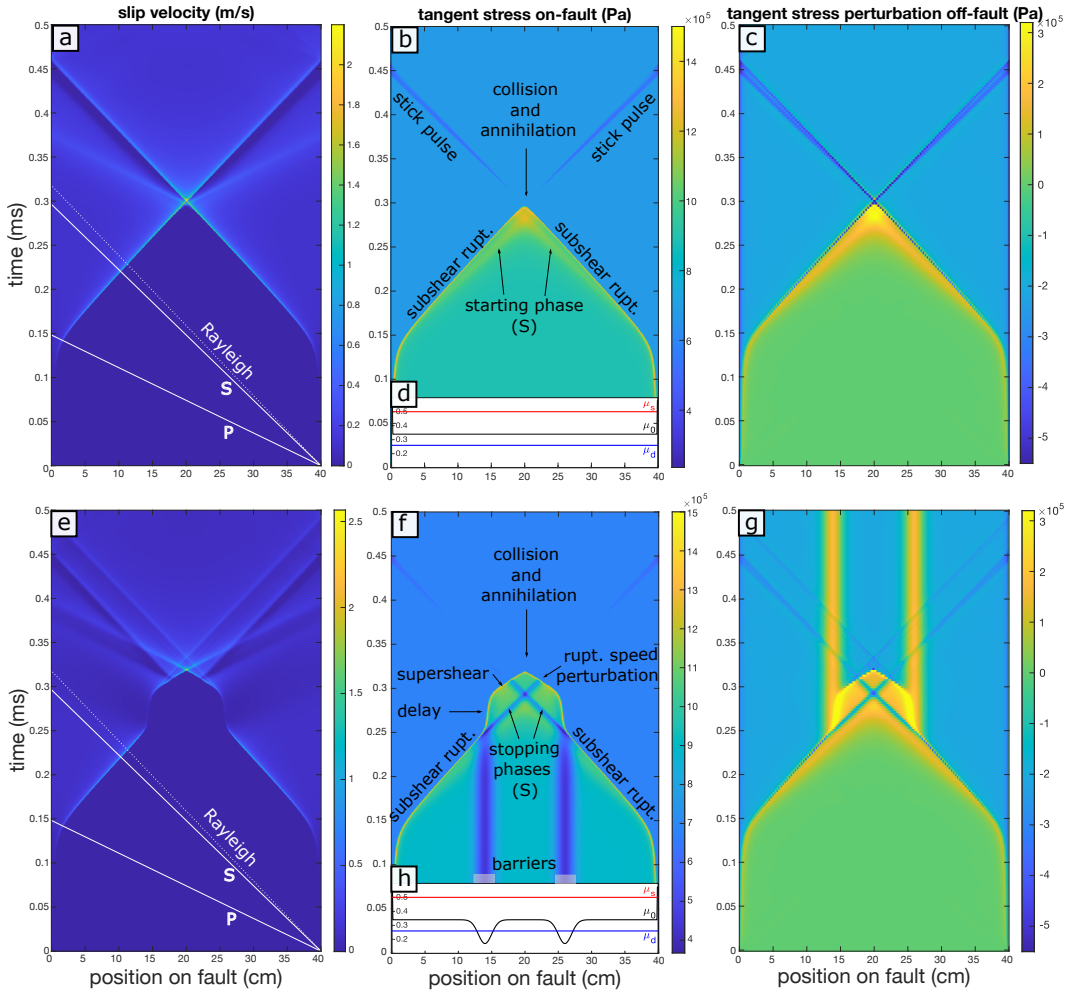

Figure 3. Numerical simulations of two ruptures colliding in two scenarios: (a,b,c,d) *homogeneous* initial shear stress and (e,f,g,h) initial shear stress with *two barriers* of low initial shear stress. For both cases, the slip-weakening friction law parameters are as follows: $\mu_s = 0.5$ (static friction); $\mu_d = 0.26$ (dynamic friction); $D_C = 1 \times 10^{-6}$ m (critical slip weakening distance). (d) and (h): initial shear stress normalized by the homogeneous normal stress (μ_0), for each case. (a) and (e): slip velocity. (b) and (f): shear stress on the fault. (c) and (g): coseismic shear stress changes at 1 mm off the fault. Lines with slopes corresponding to the P-wave speed, S-wave speed, and Rayleigh wave speed are shown for reference in (a) and (e)

eration of the rupture front, and the radiation of several phases: a peak in slip velocity propagating at the P-wave speed on the sliding part of the interface (Figure 3e), a signal propagating at the S-wave speed and another at the Rayleigh wave speed. As in the previous simulation, these interactions trigger a "stick pulse" in the last centimeters of the faults.

Finally, the two supershear rupture fronts collide, producing a phase that propagates at the P-wave speed along the fault in both directions (Figure 3e and 3g). This collision is followed by trailing Rayleigh waves, which continue to propagate even after the supershear wavefront that generated them ceases to exist.

The off-fault stress field (Figure 3g and 2b) reveals a simpler global image: the stress change is initially dominated by positive perturbations due to the starting phases, followed by negative oscillations linked to the stopping waves and trailing Rayleigh waves. The permanent stress drop associated with the supershear rupture fronts is also evident, preceding the signal due to the trailing Rayleigh wave, which only carries a transient negative stress perturbation.

In the experiment (Figure 2), the negative signals linked to the stopping waves are clearly observed, both before and after their interaction with the opposite rupture front. These signals transition from the S-wave speed to the Rayleigh wave speed upon crossing the opposite rupture front. There are no trailing Rayleigh waves in the experimental observation, because, unlike in the simulation, the ruptures do not reach a supershear velocity after their arrest. However, when the rupture fronts meet, a signal propagating at the Rayleigh wave speed is generated and propagates along the fault in both directions, similar to the first simulation when the two subshear fronts annihilate.

4 Discussion

Several points of interest emerge from this study.

First, beyond the fundamental interest in the physics of colliding fronts, this phenomenon could exist during natural earthquakes. Given the complexity of some seismic ruptures (Vallée et al., 2023; Hicks et al., 2020), rupture collisions might occur particularly during cascading ruptures (Olson & Allen, 2005; Ulrich et al., 2019).

Thanks to the high spatial and temporal resolution of our experiment, we observe that the complexity of these events generates several types of signals at higher or lower frequencies, localized on the fault. These observations align with the predictions of numerical models, allowing us to identify their nature.

The first type of signal comprises waves that propagate along the non-slipping parts of the fault. These are S-waves generated by the acceleration and deceleration of rupture fronts. Their wavelength and polarity depend on the acceleration of the rupture front. They correspond to the starting and stopping phases described theoretically by Madariaga (1977) and Fossum and Freund (1975). The theory shows that the shear stress field radiated along the fault by a suddenly starting mode II subshear crack is dominated by a peak at the S-wave front. In contrast, the P-wave front corresponds to the beginning of a slow and continuous growth of the shear stress (Madariaga, 1976). This explains why we observe the starting and stopping phases as propagating S-wave peaks along the fault and why we do not see any starting or stopping P-phases. The starting and stopping waves have also been observed by Svetlizky et al. (2016). We experimentally verify that the starting S-wave is a positive pulse and the stopping S-wave is a negative pulse (Rose, 1981). A striking feature is that the stopping pulse is narrower than the starting pulse, thus containing higher frequencies. These waves are not directly related to the collision, they are due to the changes in rupture velocity. They are also observed during events with a single rupture front (see Figure S2).

The second type comprises signals that propagate along the fault when it is already sliding. Experimentally, we observe these as negative perturbations of the near-fault shear stress, propagating at the Rayleigh-wave speed along the sliding parts of the fault. These are not ruptures, as they do not correspond to a transition from a non-slipping to a slipping state. Instead, they are stress perturbations localized around the sliding interface which we identify as interface waves (Fossum & Freund, 1975; Madariaga, 1976, 1977; Dunham & Archuleta, 2004; Dunham, 2005). These waves carry perturbations of slip along the sliding parts of the interface and are accompanied by perturbations of the stress and displacement fields in the bulk, localised near the interface. They are evanescent waves, thus the amplitude of these perturbations decreases with the distance to the interface. Let us notice, moreover, that in the framework of LEFM, they do not carry any perturbation of shear stress directly on the interface, but only in the bulk close to it, because the shear stress on the interface is imposed as a boundary condition of the problem. If

the shear stress on the sliding part of the interface is imposed as a constant value (dynamic shear strength value), then these waves propagate at the Rayleigh wave speed (Stoneley, 1924; Dunham, 2005; Valier-Brasier et al., 2012). If a constitutive law introduces a dependency of the shear stress on the slip rate *via* a rate dependant friction law (Rice et al., 2001), or on the slip *via* a cohesion law (Pyrak-Nolte & Cook, 1987), then these waves are dispersive, and their existence and propagation speed depend on their wavelength and on the parameters of the constitutive law. Consequently, the dispersion properties of interface waves can provide information on the constitutive behaviour of the fault.

In our experiment and numerical simulations, these interface waves are generated by several types of phenomena:

- (1) when two subshear ruptures collide
- (2) when a stopping wave enters an already sliding area
- (3) when a subshear rupture transitions to supershear
- (4) when a rupture interacts with the free surface of the sample at the edge of the fault.

The trailing Rayleigh wave generated by a transition to supershear (case 3) has been studied both experimentally and numerically (Xia et al., 2004; Passelègue et al., 2013; Dunham et al., 2003; Mello et al., 2016). There is also one clear observation of such a trailing Rayleigh wave in a near-field ground motion measurement during the 2002 supershear Denali earthquake (Dunham et al., 2003; Mello et al., 2014). We corroborate the existence of this phenomenon in our experiment, for example in events 8 and 9 (Figure S2).

More importantly, we show that these trailing Rayleigh pulses are one specific case of a more general phenomenon: interface waves on sliding frictional interfaces. The specific case of two ruptures propagating toward each other has allowed us to show that they can be generated by other types of dynamic complexities, specific to rupture collision (cases 1 and 2).

Case 1 (*i.e.*, colliding subshear ruptures) has been numerically described before (Fukuyama & Madariaga, 2000; Kame & Uchida, 2008). We provide here an experimental observation of these specific interface waves. Kame and Uchida (2008) point out that the seismic radiation from the coalescence resembles strongly that of a stopping wave. This could

be why the stopping waves are partly diffracted in interface waves by the rupture front when entering a sliding area (case 2).

The radiation of interface waves by the interaction of the rupture with an edge of the fault (case 4) is not studied in detail here, albeit it is clearly apparent in almost all the events (Figures 2 and S2). It has been observed and studied in detail by S. Xu et al. (2019), who call it a Fault-Interface Rayleigh Wave. Such waves have also been imaged experimentally in other experimental studies (Latour et al., 2013; Gounon et al., 2022; Schubnel et al., 2011; Shi et al., 2023), and sometimes casually called a "rupture rebound". However, given that the interface is already sliding when the rupture arrives at the edge, they are most probably interface waves rather than ruptures. Our observation, consistent with S. Xu et al. (2019), shows that they are not associated with a permanent stress drop, but rather with the passage of a temporary perturbation. The more detailed exploration of these interface waves in Ding et al. (2024) is consistent with our experimental findings about the generation of these interface waves.

Interface waves guided by faults have been proposed as good candidates to retrieve information about faults properties, due to the sensitivity of their dispersion curves to their constitutive law (Rice et al., 2001; Pyrak-Nolte et al., 1992). In the laboratory, S. Xu et al. (2019) have shown that their velocity is sensitive to the wear of the interface. Practically however, to image actual faults, it could be difficult to excite them by active source imaging. Here we show that they are generated by several dynamic rupture processes that can occur naturally during earthquakes. If they were to be identified in near-field seismograms, they could possibly give details on the faults properties or complexity.

Furthermore, our simulations show a clear interaction between the starting and stopping waves generated by a rupture and the rupture front propagating in the opposite direction. These waves locally modify the initial stress encountered by the rupture. When the rupture crosses a starting S-wave phase, it advances into a medium with increased initial stress, resulting in an acceleration of the rupture front. Conversely, when it crosses a stopping S-wave phase, it encounters a lower initial stress, temporarily reducing its speed. After the stopping wave has passed, the static stress field of the new arrested rupture, higher than the initially imposed one, imposes a new, more favorable stress state for the opposite rupture to propagate. As a result, the rupture arriving from the opposite direction in this zone tends to accelerate, as it encounters a greater stress drop.

These changes in rupture velocities due to the interaction of opposite rupture fronts could explain the emergence of high-frequency radiations during earthquakes. High frequencies are generally explained as the failure of over-stressed areas, generating larger local stress drops and higher slip rates. Our results demonstrate that similar peak slip rates and high-frequency content can also emerge from the collisions of rupture fronts or from their interaction through the stopping and starting phases they radiate.

A final interesting feature, emerging from numerical observation only, is the occurrence of a "stick pulse", the contrary of a slip pulse. It appears as a finite zone in which the slip velocity is zero, that propagates in an otherwise sliding area of the fault. Inside this zone, the on-fault shear stress is below the frictional strength, and its value is controlled by elasto-dynamics rather than friction. Slip resumes when the frictional strength is reached again. In our simulations, during arrest the friction coefficient remains unchanged, thus equal to μ_d, simulating a fault with no frictional healing. Thus the new rupture that constitutes the end of the "stick-pulse" does not carry a stress drop. In the off-fault stress field, it is difficult to distinguish between the passage of this "stick pulse" and the passage of an interface wave, as both correspond to a negative signal. The only difference is that the signal associated with the "stick-pulse" widens when propagating. It has been demonstrated in Das (2003) and further discussed in Dunham and Archuleta (2004) that the radiated wave field opposes slipping between the arrival times of the S-wave and the Rayleigh wave, while aligning with the direction of slip both before and after this interval. This behavior, when combined with our friction law, explains the occurrence of the stick-pulse observed in our simulations.

The stick pulse closely resembles secondary ruptures that have been observed in laboratory experiments (Kammer & McLaskey, 2019; Shi et al., 2023). Interestingly, in Kammer and McLaskey (2019) these secondary ruptures also appear to propagate at the Rayleigh wave velocity. As discussed in Rice et al. (2001), an interface wave of a certain wavelength can transition into a secondary rupture, associated with stress drop, when a velocity-weakening constitutive law is applied. Further exploration of interface waves and their relationship to secondary ruptures could therefore help constrain the constitutive laws of frictional interfaces.

5 Open Research

The numerical code used to simulate dynamic rupture propagation is SEM2DPACK (Ampuero, 2012), an open-source research code available at `https://github.com/jpampuero/sem2dpack`. The raw experimental data and the input files for simulations are available (Latour et al., 2024).

Acknowledgments

The authors acknowledges funding from the European Union (ERC Starting Grant HOPE num. 101041966). This research was partially funded by the program TelluS-ALEAS of CNRS-INSU (project EDRHEx). J.P.A. is supported by the French government, through the UCAJEDI Investments in the Future project (ANR-15-IDEX-01) managed by the National Research Agency (ANR). The authors thank reviewer Eric Dunham for insightful comments which greatly improved the manuscript.

References

Ampuero, J. (2012). *SEM2DPACK, a spectral element software for 2D seismic wave propagation and earthquake source dynamics, v2.3.8.* [software]. Zenodo. Retrieved from `https://doi.org/10.5281/zenodo.230363` doi: 10.5281/zenodo.230363

Beroza, G. C., & Spudich, P. (1988). Linearized inversion for fault rupture behavior: Application to the 1984 Morgan Hill, California, earthquake. *Journal of Geophysical Research: Solid Earth*, *93*(B6), 6275–6296.

Burridge, R. (1973). Admissible speeds for plane-strain self-similar shear cracks with friction but lacking cohesion. *Geophysical Journal International*, *35*(4), 439–455.

Das, S. (2003). Dynamic fracture mechanics in the study of the earthquake rupturing process: theory and observation. *Journal of the Mechanics and Physics of Solids*, *51*(11-12), 1939–1955.

Das, S., & Kostrov, B. (1983). Breaking of a single asperity: Rupture process and seismic radiation. *Journal of Geophysical Research: Solid Earth*, *88*(B5), 4277–4288.

Day, S. M. (1982). Three-dimensional simulation of spontaneous rupture: the effect of nonuniform prestress. *Bulletin of the Seismological Society of America*,

386 *72*(6A), 1881–1902.

387 Ding, X., Xu, S., Fukuyama, E., & Yamashita, F. (2024). *Back-propagating rupture:*
388 *Nature, excitation, and implications* [preprint]. Retrieved from `https://arxiv`
389 `.org/abs/2406.01286`

390 Dunham, E. M. (2005). Dissipative interface waves and the transient response
391 of a three dimensional sliding interface with Coulomb friction. *Journal*
392 *of The Mechanics and Physics of Solids*, *53*, 327-357. Retrieved from
393 `https://api.semanticscholar.org/CorpusID:15220077`

394 Dunham, E. M., & Archuleta, R. J. (2004). Evidence for a supershear transient dur-
395 ing the 2002 Denali fault earthquake. *Bulletin of the Seismological Society of*
396 *America*, *94*(6B), S256–S268.

397 Dunham, E. M., Favreau, P., & Carlson, J. (2003). A supershear transition mecha-
398 nism for cracks. *Science*, *299*(5612), 1557–1559.

399 Fossum, A., & Freund, L. (1975). Nonuniformly moving shear crack model of a
400 shallow focus earthquake mechanism. *Journal of Geophysical Research*, *80*(23),
401 3343–3347.

402 Freund, L. (1972). Crack propagation in an elastic solid subjected to general load-
403 ing — I. Constant rate of extension. *Journal of the Mechanics and Physics of*
404 *Solids*, *20*(3), 129–140.

405 Fukuyama, E., & Madariaga, R. (2000). Dynamic propagation and interaction of
406 a rupture front on a planar fault. *Pure and Applied Geophysics*, *157*(11-12),
407 1959–1979.

408 Gounon, A., Latour, S., Letort, J., & El Arem, S. (2022). Rupture nucleation on
409 a periodically heterogeneous interface. *Geophysical Research Letters*, *49*(20),
410 e2021GL096816.

411 Hicks, S. P., Okuwaki, R., Steinberg, A., Rychert, C. A., Harmon, N., Abercrombie,
412 R. E., ... others (2020). Back-propagating supershear rupture in the 2016 Mw
413 7.1 Romanche transform fault earthquake. *Nature Geoscience*, *13*(9), 647–653.

414 Kame, N., & Uchida, K. (2008, 08). Seismic radiation from dynamic coalescence,
415 and the reconstruction of dynamic source parameters on a planar fault. *Geo-*
416 *physical Journal International*, *174*(2), 696-706. Retrieved from `https://doi`
417 `.org/10.1111/j.1365-246X.2008.03849.x` doi: 10.1111/j.1365-246X.2008
418 .03849.x

Kammer, D. S., & McLaskey, G. C. (2019). Fracture energy estimates from large-scale laboratory earthquakes. *Earth and Planetary Science Letters*, *511*, 36–43.

Kostrov, B. (1964). Selfsimilar problems of propagation of shear cracks. *Journal of Applied Mathematics and Mechanics*, *28*(5), 1077–1087.

Kostrov, B. (1966). Unsteady propagation of longitudinal shear cracks. *Journal of applied Mathematics and Mechanics*, *30*(6), 1241–1248.

Latour, S., Passelègue, F., Paglialunga, F., & Noël, C. (2024). *Raw data and simulation input file for friction experiment "crack28" performed at geoazur on 2023/06/30* [dataset]. Zenodo. Retrieved from `https://doi.org/10.5281/zenodo.11519985` doi: 10.5281/zenodo.11519985

Latour, S., Schubnel, A., Nielsen, S., Madariaga, R., & Vinciguerra, S. (2013). Characterization of nucleation during laboratory earthquakes. *Geophysical Research Letters*, *40*(19), 5064–5069.

Madariaga, R. (1976). Dynamics of an expanding circular fault. *Bulletin of the Seismological Society of America*, *66*(3), 639–666.

Madariaga, R. (1977, 12). High-frequency radiation from crack (stress drop) models of earthquake faulting. *Geophysical Journal International*, *51*(3), 625-651. Retrieved from `https://doi.org/10.1111/j.1365-246X.1977.tb04211.x` doi: 10.1111/j.1365-246X.1977.tb04211.x

Mello, M., Bhat, H., Rosakis, A., & Kanamori, H. (2014). Reproducing the supershear portion of the 2002 Denali earthquake rupture in laboratory. *Earth and Planetary Science Letters*, *387*, 89-96. Retrieved from `https://www.sciencedirect.com/science/article/pii/S0012821X1300664X` doi: https://doi.org/10.1016/j.epsl.2013.11.030

Mello, M., Bhat, H. S., & Rosakis, A. J. (2016). Spatiotemporal properties of sub-Rayleigh and supershear rupture velocity fields: Theory and experiments. *Journal of the Mechanics and Physics of Solids*, *93*, 153–181.

Meng, L., Bao, H., Huang, H., Zhang, A., Bloore, A., & Liu, Z. (2018). Double pincer movement: Encircling rupture splitting during the 2015 Mw 8.3 Illapel earthquake. *Earth and Planetary Science Letters*, *495*, 164–173.

Nielsen, S., Taddeucci, J., & Vinciguerra, S. (2010, 02). Experimental observation of stick-slip instability fronts. *Geophysical Journal International*, *180*(2), 697-702.

doi: 10.1111/j.1365-246X.2009.04444.x

Olson, E. L., & Allen, R. M. (2005). The deterministic nature of earthquake rupture. *Nature*, *438*(7065), 212–215.

Paglialunga, F., Passelègue, F., Latour, S., Gounon, A., & Violay, M. (2023). Influence of viscous lubricant on nucleation and propagation of frictional ruptures. *Journal of Geophysical Research: Solid Earth*, *128*(4), e2022JB026090. Retrieved from `https://agupubs.onlinelibrary.wiley.com/doi/abs/10.1029/2022JB026090` (e2022JB026090 2022JB026090) doi: https://doi.org/10.1029/2022JB026090

Passelègue, F. X., Schubnel, A., Nielsen, S., Bhat, H. S., & Madariaga, R. (2013). From sub-Rayleigh to supershear ruptures during stick-slip experiments on crustal rocks. *Science*, *340*(6137), 1208–1211.

Pyrak-Nolte, L. J., & Cook, N. G. W. (1987). Elastic interface waves along a fracture. *Geophysical Research Letters*, *14*(11), 1107-1110. Retrieved from `https://agupubs-onlinelibrary-wiley-com.gorgone.univ-toulouse.fr/doi/abs/10.1029/GL014i011p01107` doi: https://doi-org.gorgone.univ-toulouse.fr/10.1029/GL014i011p01107

Pyrak-Nolte, L. J., Xu, J., & Haley, G. M. (1992). Elastic interface waves propagating in a fracture. *Physical review letters*, *68*(24), 3650.

Ravi-Chandar, K. (2004). *Dynamic fracture*. Elsevier.

Rice, J. R., Lapusta, N., & Ranjith, K. (2001). Rate and state dependent friction and the stability of sliding between elastically deformable solids. *Journal of the Mechanics and Physics of Solids*, *49*(9), 1865–1898.

Rose, L. (1981). The stress-wave radiation from growing cracks. *International Journal of Fracture*, *17*, 45–60.

Schubnel, A., Nielsen, S., Taddeucci, J., Vinciguerra, S., & Rao, S. (2011). Photo-acoustic study of subshear and supershear ruptures in the laboratory. *Earth and Planetary Science Letters*, *308*(3-4), 424–432. doi: https://doi.org/10.1016/j.epsl.2011.06.013

Shi, S., Wang, M., Poles, Y., & Fineberg, J. (2023). How frictional slip evolves. *Nature communications*, *14*(1), 8291.

Stoneley, R. (1924). Elastic waves at the surface of separation of two solids. *Proceedings of the Royal Society of London. Series A, Containing Papers of a*

Mathematical and Physical Character, *106*(738), 416–428.

Svetlizky, I., & Fineberg, J. (2014). Classical shear cracks drive the onset of dry frictional motion. *Nature*, *509*(7499), 205–208.

Svetlizky, I., Pino Muñoz, D., Radiguet, M., Kammer, D. S., Molinari, J.-F., & Fineberg, J. (2016). Properties of the shear stress peak radiated ahead of rapidly accelerating rupture fronts that mediate frictional slip. *Proceedings of the National Academy of Sciences*, *113*(3), 542–547.

Ulrich, T., Gabriel, A.-A., Ampuero, J.-P., & Xu, W. (2019). Dynamic viability of the 2016 Mw 7.8 Kaikōura earthquake cascade on weak crustal faults. *Nature communications*, *10*(1), 1213.

Valier-Brasier, T., Dehoux, T., & Audoin, B. (2012, 07). Scaled behavior of interface waves at an imperfect solid-solid interface. *Journal of Applied Physics*, *112*(2), 024904. Retrieved from `https://doi.org/10.1063/1.4733949` doi: 10.1063/1.4733949

Vallée, M., Xie, Y., Grandin, R., Villegas-Lanza, J. C., Nocquet, J.-M., Vaca, S., ... others (2023). Self-reactivated rupture during the 2019 Mw= 8 northern Peru intraslab earthquake. *Earth and Planetary Science Letters*, *601*, 117886.

Wang, T. A., Dunham, E. M., Krenz, L., Abrahams, L. S., Segall, P., & Yoder, M. R. (2024). Dynamic rupture simulations of caldera collapse earthquakes: Effects of wave radiation, magma viscosity, and evidence of complex nucleation at Kılauea 2018. *Journal of Geophysical Research: Solid Earth*, *129*(4), e2023JB028280.

Xia, K., Rosakis, A. J., & Kanamori, H. (2004). Laboratory earthquakes: The sub-Rayleigh-to-supershear rupture transition. *Science*, *303*(5665), 1859–1861.

Xu, L., Ji, C., Meng, L., Ampuero, J.-P., Yunjun, Z., Mohanna, S., & Aoki, Y. (2024). *Dual-initiation ruptures in the 2024 noto earthquake encircling a fault asperity at a swarm edge* (Vol. 385) (No. 6711). Retrieved from `https://www.science.org/doi/abs/10.1126/science.adp0493` doi: 10.1126/science.adp0493

Xu, S., Fukuyama, E., Yamashita, F., & Takizawa, S. (2019). Evolution of Fault-Interface Rayleigh Wave speed over simulated earthquake cycles in the lab: Observations, interpretations, and implications. *Earth and Planetary Science Letters*, *524*, 115720. Retrieved from `https://www.sciencedirect.com/`

518 science/article/pii/S0012821X19304121 doi: https://doi.org/10.1016/
519 j.epsl.2019.115720